10 March 1995

ELSEVIER

Chemical Physics Letters 234 (1995) 416–424

CHEMICAL PHYSICS LETTERS

Quantum effects on the structure and energy of a protonated linear chain of hydrogen-bonded water molecules

Régis Pomès, Benoît Roux

Department of Chemistry, University of Montreal, C.P. 6128, Succ. A, Montreal, Quebec, Canada H3C 3J7

Received 8 October 1994; in final form 12 December 1994

Abstract

Computer simulations of a protonated, linear cluster of four hydrogen-bonded water molecules, $(O_4H_9)^+$, are reported. The potential energy surface governing the motion of the nuclei was described with the polarization model of Stillinger and co-workers. The quantization of all the hydrogen nuclei was treated with the discretized Feynman path integral formalism. Results indicate that quantum dispersion has a significant influence on the conformational fluctuations of the system at 300 K. Configurations in which the energy profile of the central proton along the transfer coordinate possesses a single- or double-well character occur spontaneously due to thermal fluctuations.

1. Introduction

The role of water molecules in mediating the transfer of protons is of fundamental importance in the function of a number of biological systems. There is considerable evidence that the fast translocation of protons over large distances may take place in several systems along a linear chain of hydrogen-bonded water molecules, or 'proton wire' [1]. For example, such a mechanism was proposed to account for the fast conduction of protons across transmembrane pores such as the gramicidin channel, which can occur at rates one to two orders of magnitude higher than those of other cations [2]. A similar mechanism has been proposed to account for the rapid transfer of a proton over a distance of 10–12 Å in the last steps of the photocycle of the light-driven proton pump bacteriorhodopsin [3–5].

Given the importance of proton wires in biology, it is desirable to gain more information on their properties using computational models. The characterization of proton transfers in such a complex environment as a hydrogen-bonded water chain is a challenging problem due to a combination of two different factors. First, it is essential to take rigorously into account the quantum mechanical nature of the proton and its manifestation in terms of zero point vibration and tunneling. Second, for a meaningful study it is important to use an accurate and realistic description of the Born–Oppenheimer potential surface governing the motions of the nuclei in the hydrogen-bonded water chain. Extensive calculations dedicated to the characterization of the geometry of small proton hydrates, $(H_2O)_nH^+$, indicate that the potential energy surface of these small clusters is very sensitive to the details of the ab initio method [6–11]. In particular, the calculations showed that the potential surface of $(H_2O)_2H^+$ is strongly anharmonic and has many local minima [6,7,12,13]. The significant structural flexibility of small proton hydrates [11,14] suggest that thermal fluctuations can lead to considerable distortion of the geometry of the

SSDI 0009-2614(95)00071-2

proton wire and large variation in the energy barriers opposing proton transfer from donor to acceptor. Despite their interest from a fundamental point of view, most previous theoretical studies of proton transfer were based on simplified model systems and do not provide a realistic description of proton transfer along a flexible water chain. At the present time, the interplay between the quantum mechanical effects and the strong and complex anharmonic character of the potential energy surface has not been explored for such systems.

The main objective of this study is to investigate the importance of quantum effects on the structural fluctuations of a linear hydrogen-bonded water chain at room temperature. We present results from quantum and classical molecular dynamics simulations for a linear, protonated cluster of four water molecules, $(H_2O)_4H^+$. The potential energy surface governing the motion of the nuclei was modeled with the polarization model (PM6) of Weber and Stillinger [15]. The effects arising from the quantization of the hydrogen nuclei were treated with discretized Feynman path integrals [16]. The structural properties of the linear hydrogen-bonded network are analyzed. The potential of mean force for the motion of the excess proton at the center of the hydrogen-bonded network is calculated. The observed properties of the flexible hydrogen-bonded chain are contrasted to previous theoretical studies of proton transfer based on simplified model systems. An important aspect of the present simulations is that the quantization of all nine proton nuclei along the water chain is taken into account in the path integral simulations. To our knowledge, this study is one of the first attempts to describe a proton-transfer system in a quantum, protic environment using a realistic potential energy surface.

2. Method

This section starts with an overview of the potential energy function devised to represent water molecules in the PM6 model; we then discuss the implementation of that model in the discretized Feynman path integral approach used to account for quantum effects involving hydrogen nuclei; we end with a brief description of the methodology employed to generate trajectories and to compute free energy profiles and other properties of the system.

The PM6 version of the polarization model developed by Stillinger and co-workers [15,17,18] was used to approximate the potential energy surface of the $(H_2O)_4H^+$ cluster. The PM6 model energy function was developed and parametrized to accurately reproduce the structure and energy of small hydrogen bonded cationic and anionic water clusters. In contrast with rigid [19,20] or partially flexible water models [21], the basic structural elements of PM6 are H^+ and O^{2-} atoms, which makes it possible to account for the full dissociation of water molecules into ionic fragments. The basic structural elements of PM6 are O^{2-} and H^+ atoms. For a configuration of the oxygen and hydrogen constituents with coordinates $\{r_O\} = \{r_{O_1}, \ldots, r_{O_4}\}$ and $\{r_H\} = \{r_{H_1}, \ldots, r_{H_9}\}$, the PM6 potential energy is [15]

$$
\begin{aligned}
U(\{r_O\}, \{r_H\}) &= \sum_{i<j=1}^{N_O} \phi_{OO}\left(|r_{O_i} - r_{O_j}|\right) \\
&\quad + \sum_{i=1}^{N_O}\sum_{j=1}^{N_H} \phi_{OH}\left(|r_{O_i} - r_{H_j}|\right) \\
&\quad + \sum_{i<j=1}^{N_H} \phi_{HH}\left(|r_{H_i} - r_{H_j}|\right) \\
&\quad + \Phi_{pol}(\{r_O\}, \{r_H\}), \qquad (1)
\end{aligned}
$$

where ϕ_{OO}, ϕ_{OH} and ϕ_{HH} are pair-wise radially symmetric functions and Φ_{pol} represents a many-body polarization energy contribution resulting from the polarization of the oxygen particles that must be determined self-consistently.

To illustrate the features of the PM6 model, we briefly compare the properties of the protonated water dimer, $(O_2H_5)^+$, obtained with the PM6 model with those obtained by ab initio calculations using the 4-31G basis set at the Hartree–Fock level [22,23]. In the optimized PM6 configuration, the oxygen–oxygen distance is 2.47 whereas it is 2.37 Å in the ab initio calculations. In both cases, the central proton lies half-way between the two oxygens and the energy profile along the oxygen–oxygen axis has a single minimum. A double well separated by an energy barrier appears for larger oxygen–oxygen

separation and the height of the barrier increases sharply as a function of oxygen–oxygen separation. Ab initio calculations performed with the 4-31G basis set using the GAUSSIAN 90 program [24] indicate that the barrier is 2.61 kcal/mol for an oxygen–oxygen separation of 2.59 Å, whereas it is 3.01 kcal/mol with the PM6 model. For larger separations, the barrier rises more rapidly with the PM6 model than in ab initio calculations. Nevertheless, the PM6 model reproduces the qualitative features of the ab initio potential essential to the transfer of the central proton, namely, the existence of a potential energy barrier and its dependence on the oxygen–oxygen separation.

The importance of quantum effects was investigated by exploiting the isomorphism of the discretized Feynman path integral representation of the density matrix with an effective classical system obeying Boltzmann statistics [16]. Only the quantization of the protons was considered and the oxygens were treated as classical particles. Following the path integral approach, each proton was replaced in the effective classical system by a ring polymer, or necklace, of P fictitious particles with a harmonic spring between nearest neighbors along the ring. The potential energy of the effective classical system is

$$U_{\mathrm{eff}}\left(\{\boldsymbol{r}_{\mathrm{O}}\},\{\boldsymbol{r}_{\mathrm{H}}^{(1)}\},\ldots,\{\boldsymbol{r}_{\mathrm{H}}^{(P)}\}\right) = \frac{1}{P}\sum_{p=1}^{P} U\left(\{\boldsymbol{r}_{\mathrm{O}}\},\{\boldsymbol{r}_{\mathrm{H}}^{(p)}\}\right) + \sum_{i=1}^{N_{\mathrm{H}}}\sum_{p=1}^{P} \tfrac{1}{2}K_{\mathrm{polymer}}\,|\,\boldsymbol{r}_{\mathrm{H}_i}^{(p)} - \boldsymbol{r}_{\mathrm{H}_i}^{(p+1)}\,|^2, \qquad (2)$$

where $\{\boldsymbol{r}_{\mathrm{H}}^{(p)}\} = \{\boldsymbol{r}_{\mathrm{H}_1}^{(p)},\ldots,\boldsymbol{r}_{\mathrm{H}_9}^{(p)}\}$ represents the coordinates of the pth particle for protons H_1–H_9, and $K_{\mathrm{polymer}} = PM_{\mathrm{H}}k_{\mathrm{B}}T/\hbar^2$ is the harmonic spring constant acting between the pth and $(p+1)$th nearest neighbors along the polymer necklace representing each proton H_i of mass M_{H}. Note that in the second summation of Eq. (2), $P+1 \equiv 1$ is required so as to satisfy the closure of the ring polymers. In the present path integral simulations, each proton was represented as a polymer necklace of $P = 32$ fictitious particles, yielding a total of 292 particles in the effective system. This contrast with previous path integral simulations of water in which only three fictitious particles per hydrogen were used to study the quantization of the rotational and librational motions of rigid water models [25]. A much larger number is necessary in the present study because high frequency bond stretching modes are included. A discretization of the path integral with 20 to 30 fictitious particles was found to be adequate in recent path integral studies of proton transfer in model systems [26–28].

The configurational sampling was performed by generating Langevin molecular dynamics trajectories of the effective system. For all degrees of freedom x_α in the effective classical system, the trajectory was calculated according to the Langevin equation of motion,

$$m_\alpha \ddot{x}_\alpha = -\partial_{x_\alpha} U_{\mathrm{eff}} - \gamma \dot{x}_\alpha + f(t), \qquad (3)$$

where γ is a friction constant and $f(t)$ is a random gaussian force obeying the fluctuation–dissipation theorem,

$$\langle f(t) f(0)\rangle = 2k_{\mathrm{B}}T\gamma\delta(t), \qquad (4)$$

insuring that the configurations were generated according to a Boltzman distribution, $\exp[-U_{\mathrm{eff}}/k_{\mathrm{B}}T]$, at temperature T. It should be emphasized that the resulting Boltzmann distribution is independent of the choice of dynamical mass m_α attributed to each degree of freedom. The choice of Langevin dynamics was dictated by the need to avoid the nonergodicity of path integral simulations based on molecular dynamics with thermostats [29].

During the trajectories of the effective system, the full PM6 potential function, $U(\{\boldsymbol{r}_{\mathrm{O}}\},\{\boldsymbol{r}_{\mathrm{H}}^{(p)}\})$ was recalculated for each p-step of the discretized path integral. In particular, the interactions involving the pair-wise interactions ϕ_{HH} and ϕ_{OH} were re-calculated. It is important to note that the polarization energy contribution, $\Phi_{\mathrm{pol}}(\{\boldsymbol{r}_{\mathrm{O}}\},\{\boldsymbol{r}_{\mathrm{H}}^{(p)}\})$, was determined by solving a set of self-consistent equations for each value of p. In other words, each molecular dynamics time-step involved the determination of 32 polarization states induced on the four oxygen atoms. The forces on all particles due to the many-body polarization were calculated analytically by solving a similar set of self-consistent equations derived by Stillinger [17]. Other contributions arising from constant terms, such as the oxygen–oxygen ϕ_{OO} interaction, were calculated only once and stored for computational efficiency.

Molecular dynamics simulations were performed on a protonated linear chain of four water molecules, $(O_4H_9)^+$, using the method described above. For the sake of comparison, the simulations were repeated in the classical limit, which corresponds to $P = 1$. The energy-optimized conformation of the chain was used as a starting point. During the course of the simulations, a harmonic restoring potential was applied to the oxygen lying beyond 1.5 Å from the axis of the linear chain. This cylindrical restoring potential was used to model the channel environment of the proton wire and to maintain the linearity of the chain. The trajectories were generated at 300 K with a modified version of the CHARMM program [30] using Langevin dynamics with a time-step of 0.5 fs. A dynamical mass corresponding to the mass of a proton was assigned to each p-proton in the ring polymers. A friction coefficient γ corresponding to a velocity relaxation time of 0.2 ps was assigned to all the particles in the effective system. After equilibration, 2 ns simulations were produced for both the classical and the effective quantum systems. The coordinates of the system were recorded every 100 steps for analysis.

In order to evaluate the influence of proton motion on the structure of the chain, two-dimensional separation distribution functions $\rho(R, r)$ were computed, where R and r are respectively the oxygen–oxygen and the proton–oxygen separations for the central hydrogen bond. In the quantum case, the distribution function was calculated as an average over the P configurations of the discretized path integral,

$$\rho(R, r) = \left\langle \frac{1}{P} \sum_{p=1}^{P} \delta\left(| \boldsymbol{r}_{O_2} - \boldsymbol{r}_{O_3} | - R \right) \times \delta\left(| \boldsymbol{r}_{O_2} - \boldsymbol{r}_{H_a}^{(p)} | - r \right) \right\rangle . \quad (5)$$

The topological symmetry around the center of the tetrameric chain was used to improve the convergence of the statistical sampling. The potential of mean force (PMF), $\mathscr{W}(R, r)$, relative to the global minimum was obtained from the distribution $\rho(R, r)$ using $\mathscr{W}(R, r) = -k_B T \ln[\rho(R, r)]$.

The analysis of the spatial dispersion of protons was carried out through the calculation of the radius of gyration of each ring polymer H_i,

$$\mathscr{R}_{H_i}^{gyr} = \left\langle \frac{1}{P} \sum_{p=1}^{P} \| \boldsymbol{r}_{H_i}^{(p)}(t) - \bar{\boldsymbol{r}}_{H_i}(t) \|^2 \right\rangle^{1/2} , \quad (6)$$

where averaging runs over the entire simulation time of 2 ns, and $\bar{\boldsymbol{r}}_{H_i}(t) = (1/P)\sum_{p=1}^{P} \boldsymbol{r}_{H_i}^{(p)}(t)$ corresponds to the position of the centroid of ring polymer H_i at time t.

The quantum energy levels corresponding to the motion of the proton along the central hydrogen bond were computed by solving the one-dimensional Schrödinger equation for the potential energy profile $U(r)$,

$$-\frac{\hbar}{2M_H}\psi''(r) + U(r)\psi(r) = E\psi(r). \quad (7)$$

The one-dimensional potential energy profile $U(r)$ was calculated from a given configuration of the chain by moving the central proton along the oxygen–oxygen axis at a distance r from one of the oxygen atoms. All other degrees of freedom fixed were held fixed. The one-dimensional Schrödinger equation was solved numerically by using basis sets constructed from the lowest eigenstates of the particle in a square well potential of width L, namely, functions of $\sin(n\pi r/L)$, where n is a non-zero integer. The potential was assumed to be infinite for $r \leqslant r_0$ and $r \geqslant r_0 + L$. The choices of $r_0 = 0.8$ Å, $L = 1.0$ Å, and $1 \leqslant n \leqslant 10$ were found to be appropriate for the calculation.

3. Results and discussion

The system is depicted schematically in Fig. 1. The presence of an extra proton induces a strong, short hydrogen bond at the center of the oligomer. In

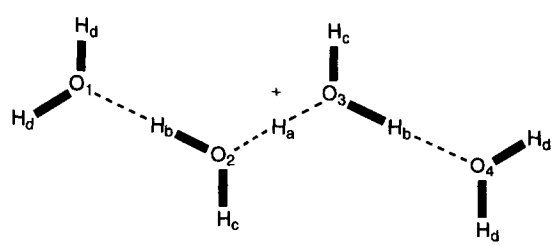

Fig. 1. Linear, protonated chain of four water molecules.

the minimum energy configuration, there is no intrinsic barrier to proton motion along this symmetric bond. Around the central hydrogen bond, the donor–acceptor pattern inverts into acceptor–donor. While the PM6 model predicts an optimized oxygen–oxygen separation of 2.90 Å for the gas-phase water dimer [17], hydrogen bond distances in the chain are affected by the net positive charge of the excess proton. As listed in Table 1, the central bond is shortest at separations in the vicinity of 2.50 Å, while the end bonds have intermediate lengths of about 2.70 Å. The inclusion of temperature and quantum effects alters the geometry of $(O_4H_9)^+$. Comparison of the columns of Table 1 shows a systematic increase of 0.02 Å for the end hydrogen bonds to 0.04 Å for the central hydrogen bond going from optimized to average classical. Likewise, there is an increase of 0.02–0.03 Å in the average quantum hydrogen bond lengths with respect to the average classical hydrogen bond lengths. The average radius of gyration of the ring polymer, calculated using Eq. (6), is given in Table 1. The greater forces acting on the protons involved in hydrogen bonds, labeled H_a and H_b in Fig. 1, relative to that imposed on their dangling counterparts, H_c and H_d, is reflected in a consistently smaller radius of gyration of 0.14 and 0.15 Å, compared to about 0.16 Å for H_c and H_d. This translates into an average diameter of 0.28 Å for the central proton, a value consistent with the width of the potential energy barrier opposed to the motion of proton, typically, at hydrogen bond lengths of about 2.60 Å. In the following discussion, the coupling of the central proton coordinate to oxygen–oxygen separations is investigated in more detail.

Table 1
Geometry of the hydrogen-bonded chain. Top: O–O separations obtained from energy minimization, and from molecular dynamics trajectories obtained successively in the classical limit and with the path integral treatment. rms fluctuations are given in parentheses. Bottom: Radii of gyration of the path integral ring polymers. All values are in Å. See Fig. 1 for atomic labels

Properties	Optimized	Classical	Quantum
O–O separations			
O_1–O_2	2.70	2.72 (0.07)	2.74 (0.08)
O_2–O_3	2.46	2.50 (0.06)	2.53 (0.05)
O_3–O_4	2.70	2.72 (0.07)	2.74 (0.09)
radii of giration			
H_a	–	–	0.141
H_b	–	–	0.150
H_c	–	–	0.158
H_d	–	–	0.164

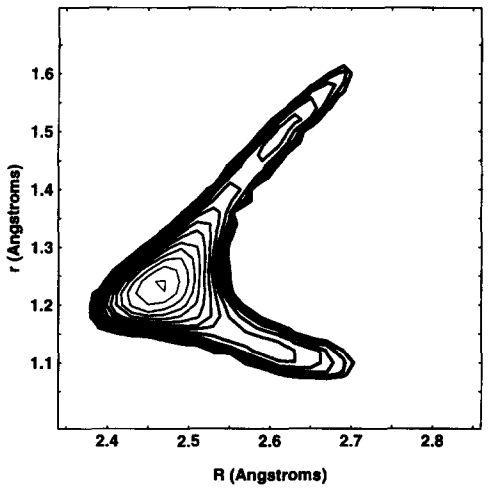

Fig. 2. Two-dimensional potential of mean force $\mathscr{W}(R, r)$ for the classical motion of a proton in a linear, hydrogen-bonded chain of four water molecules. In this figure and Fig. 3, r and R represent the central proton–oxygen and the central oxygen–oxygen separations, respectively; contours are spaced by 0.2 kcal/mol.

Two-dimensional potentials of mean force (PMF) for proton motion along the central hydrogen bond obtained respectively from classical and quantum simulations of linear $(O_4H_9)^+$ are shown in Figs. 2 and 3. Classically (Fig. 2), the proton is restricted to three well-defined minima and its position along the hydrogen bond depends strongly on the oxygen–oxygen separation. The global minimum corresponds to a short, strong 2.46 Å hydrogen bond in which the proton is located halfway between the two oxygen centers in a broad, single well. As the hydrogen bond length increases, the well splits into two equivalent minima of higher energy (relative to the global minimum). Each of these secondary minima corresponds to a weaker, 2.60 Å hydrogen bond in which the proton associates with one of the off-central oxygen atoms. The barrier separating the two secondary wells at a given oxygen–oxygen separation rises sharply with increasing hydrogen bond length. In the light of these observations, one expects that the transfer of the central proton couples strongly to

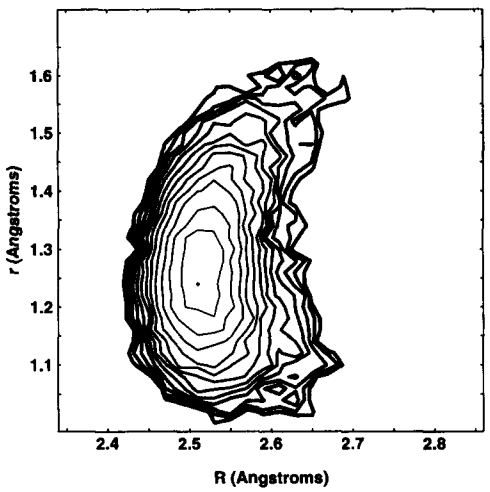

Fig. 3. Two-dimensional potential of mean force for the quantum motion of a proton in a linear, hydrogen-bonded chain of four water molecules, calculated using Eq. (7).

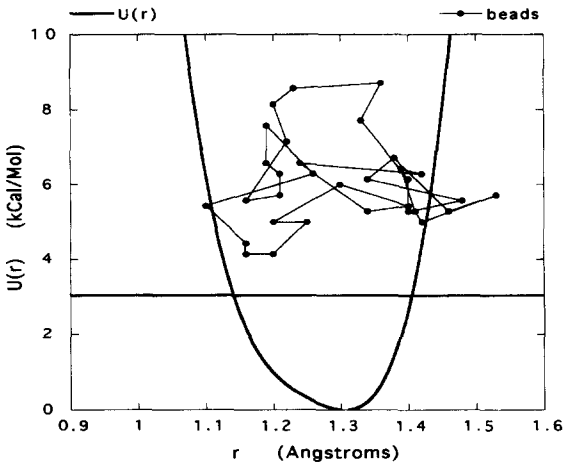

Fig. 4. Potential energy profile $U(r)$, where r is the distance between O_2 and H_a, obtained from a molecular dynamics simulation. A projection of the ring polymer representing the central proton H_a is shown for illustration. In this example the central hydrogen bond length O_2–O_3 is $R = 2.51$ Å.

successive fluctuations of the donor–acceptor distance in the classical limit.

The quantum potential of mean force shown in Fig. 3 differs dramatically from its classical counterpart. There is a striking broadening and flattening of the global minimum well, and the secondary minima disappear. The contours of the PMF calculated with the path integral simulations are broadened due to the finite radius of gyration of the polymer necklace. This corresponds to quantum dispersion effects arising from a combination of tunneling and zero-point vibration of the proton. Penetration in classically forbidden regions of the potential energy wells also contributes to the broadening of the PMF contours. The importance of such effects in the context of model hydrogen bonds has been noted by other authors [27,31].

Because of its importance to the mechanism of proton transfer between two water molecules, the character of the energy profile of the central proton along the oxygen–oxygen axis is of particular interest. Accessible hydrogen bond lengths in the quantum simulations range from 2.46 to 2.59 Å. The absolute minimum is located at an oxygen–oxygen separation of 2.52 Å. Whereas there is a single minimum for an oxygen–oxygen distance smaller than 2.52 Å, there are two energy wells separated by a barrier in the case of larger distances. At $R = 2.60$ Å, the barrier is typically 3 kcal/mol in height and about 0.3 Å in width. Two instantaneous configuration of the system, involving central oxygen–oxygen separations of $R = 2.51$ Å and $R = 2.59$ Å, were chosen to illustrate the single- and double-well cases, respectively. The corresponding potential energy for motion of the excess proton along the central hydrogen bond, $U(r)$, is shown in Figs. 4 and 5. We first note the asymmetry of the potential energy profile, a

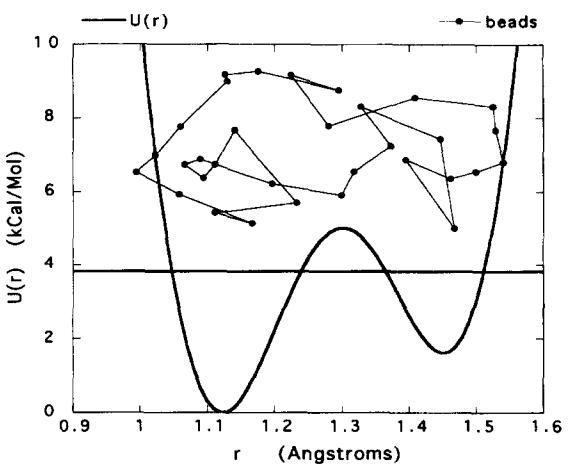

Fig. 5. Same as in the previous figure; in this example the central hydrogen bond length is $R = 2.59$ Å.

consequence of the asymmetry of the chain beyond the central hydrogen bond. The zero-point energy of the proton in this one-dimensional potential, calculated by solving the Schrödinger equation (7), is shown. The zero-point energy is in both cases larger than 3 kcal/mol. The projection of the ring polymer necklaces, representing the excess proton on a plane containing the hydrogen bond axis, are also depicted in Figs. 4 and 5. In the double-well case (Fig. 5), the polymer necklace of the central proton is delocalized over a distance of approximately 0.5 Å. It extends into both wells along the transfer coordinate r and some sections lie in the classically forbidden barrier region. Calculations of the first excited energy levels indicate that they are 5.9 and 2.7 kcal/mol higher than the ground state, respectively, in the cases depicted in Figs. 4 and 5, suggesting that the system is dominated by the ground state.

Interestingly, we note that the double-well case shown in Fig. 5, at $R = 2.59$ Å, illustrates the upper limit of accessible oxygen–oxygen distances among the equilibrium configurations of $(O_4H_9)^+$, according to the PMF contours depicted in Fig. 3. Because of the sensitivity of the barrier height upon the hydrogen bond length, probable configurations of the proton wire thus involve alternatively a single- or double-well energy profile along the transfer coordinate. In the latter case, situations in which the barrier height is smaller than or comparable to the zero-point energy of the proton nucleus can occur. Thus, the character of the proton transfer along the central bond at room temperature depends on the fluctuations in donor–acceptor separation which are themselves strongly coupled to quantum disperson effects.

Our results indicate that the structure corresponding to the energy minimum does not provide a sound basis for understanding the dynamics of the present system. Differences in the geometry of the hydrogen-bonded chain arising from the inclusion of classical dynamical effects with respect to the energy-minimized structure reflect the anharmonicity of the potential energy surface and the existence of multiple wells. The further increase in hydrogen bond lengths in the quantum case arises from the combined effects of tunneling and zero-point vibrational energy. As a consequence, the shape of the quantum PMF well is very anharmonic compared to the intrinsic potential energy profile. This strong anharmonicity cautions against the calculations of zero-point energy correction based on a harmonic approximation around the minimum energy structure. As noted by other authors, development based on the classical free energy surfaces may also not be valid [27,28]. Although these results depend, in part, on the PM6 model, we believe that the model retains the essential features of the potential energy surface (see the discussion in Section 2). Because it is important to sample a large number of configurations for meaningful studies, empirical potential functions such as PM6 represent a necessary compromise at the present time. It should be stressed that the potential energy of proton hydrates remains very difficult to characterize accurately, even with high-level ab initio calculations. Extensive calculations have indicated that the results have a significant dependence on the basis set used [6,10,23]; effects due to electron correlation, considered with Møller–Plesset perturbation theory or with configuration interaction, are also important [12,13,23].

This study has implications for the mechanism of proton transfer between hydrogen-bonded water molecules. The dominant factors controlling the proton transfer along hydrogen bonds are emerging from a number of theoretical and computational studies on model systems. Those involve mostly quantum effects arising from vibrational energy and tunneling through potential energy barriers. In addition, modulation of the potential energy profile along the hydrogen bond axis by a polar environment are also important. In cases where the hydrogen bond is relatively weak, the occurrence of proton transfer may necessitate tunneling of the proton through the substantial energy barrier. A number of recent studies have addressed such cases with model systems [26–28,31–37]. In intermediate cases where there is a small to moderate intrinsic barrier opposing the transfer, zero-point energy and thermal activation of the proton could also significantly contribute to the mechanism [27]. Finally, the intrinsic potential energy profile along strong hydrogen bonds presents no barrier to the proton motion and the influence of the surrounding solvent is dominant [28,33]. The present results based on a realistic potential contrast with studies based on model systems in which the donor–acceptor separation was either fixed or restrained to small variations. In the linear hydrogen-

bonded water chain, the donor–acceptor separation is strongly coupled to the motion of the central proton. Due to this strong coupling, the accessible configurations of the system are significantly affected by the inclusion of quantum dispersion effects. Because the energy profile for the motion of the central proton is very sensitive to the donor–acceptor separation, configurations in which the barrier is alternatively moderate, small or absent occur spontaneously under the influence of thermal fluctuations. Thus, the present study underlines the interdependence of the factors controlling the dynamics of proton transfer along hydrogen bonded water chains.

4. Conclusions

Quantum and classical simulations of linear $(O_4H_9)^+$ were performed with the PM6 model. The geometry of the water chain is influenced by the inclusion of thermal and quantum effects, and the quantization of the proton nuclei dramatically affects the PMF surface governing the motion of the central proton. These results underline the importance of quantum dispersion on a system governed by a very anharmonic potential.

The feasibility of path integral simulations based on a many-body potential being demonstrated, it will be possible to explore the properties of the proton wire using better and more accurate potential functions. In the meantime, we believe that the present model constitutes a useful tool to address questions pertaining to the mechanism of proton transfer along hydrogen-bonded chains of water molecules. In that perspective, a more systematic study is in progress [38], in which the combined effects of chain length, proton tunneling, proton–proton correlation, and of the quantization of the vibrational energy of the proton will be investigated in greater detail. This method will then be extended to the simulation of proton transfer processes across proton wires in biological systems.

Acknowledgement

This work was supported by a grant from the Medical Research Council of Canada.

References

[1] J.F. Nagle and S. Tristam-Nagle, J. Membrane Biol. 74 (1983) 1.
[2] D.W. Deamer and J.W. Nichols, J. Membrane Biol. 107 (1989) 91.
[3] R. Henderson, J.M. Baldwin, T.A. Ceska, F. Zemlin, E. Beckmann and K.H. Downing, J. Mol. Biol. 213 (1990) 899.
[4] Y. Cao, G. Váró, M. Chang, B. Ni, R. Needleman and J.K. Lanyi, Biochemistry 30 (1991) 10972.
[5] M. Ferrand, G. Zaccai, M. Nina, J.C. Smith, J.C. Etchebest and B. Roux, Fed. Eur. Biochem. Soc. 327 (1993) 256.
[6] H.Z. Cao, M. Allavena, O. Tapia and E.M. Evleth, J. Phys. Chem. 89 (1985) 1581.
[7] S. Scheiner, Accounts Chem. Res. 18 (1985) 174.
[8] M.A. Muñiz, J. Bertrán, J.L. Andrés, M. Duran and A. Lledós, J. Chem. Soc. Faraday Trans. I 81 (1985) 1547.
[9] E. Kochanski, Chem. Phys. Letters 133 (1987) 143.
[10] L.I. Yeh, M. Okumura, J.D. Myers, J.M. Price and Y.T. Lee, J. Chem. Phys. 91 (1989) 7319.
[11] T. Komatsuzaki and I. Ohmine, Chem. Phys. 180 (1994) 239.
[12] Z. Latajka and S. Scheiner, J. Molec. Struct. THEOCHEM 234 (1991) 373.
[13] M.J. Frisch, J.E. Del Bene, J.S. Binkley and H.F. Schaeffer III, J. Chem. Phys. 84 (1986) 2279.
[14] A. Potier, J.M. Leclerq and M. Allavena, J. Phys. Chem. 88 (1984) 1125.
[15] T.A. Weber and F.H. Stillinger, J. Phys. Chem. 86 (1982) 1314.
[16] D. Chandler and P.G. Wolynes, J. Chem. Phys. 74 (1981) 4078.
[17] F.H. Stillinger and C.W. David, J. Chem. Phys. 69 (1978) 1473.
[18] F.H. Stillinger, J. Chem. Phys. 71 (1979) 1647.
[19] A. Rahmouni, E. Kochanski, R. Wiest, P.E.S. Wormer and J. Langlet, J. Chem. Phys. 93 (1990) 6648.
[20] R.E. Kozack and P.C. Jordan, J. Chem. Phys. 96 (1992) 3131.
[21] S.-B. Zhu, S. Singh and G.W. Robinson, J. Chem. Phys. 95 (1991) 2791.
[22] S. Scheiner, J. Am. Chem. Soc. 103 (1981) 315.
[23] S. Scheiner, M.M. Szcześniak and L.D. Bingham, Intern. J. Quantum Chem. 23 (1983) 739.
[24] M.J. Frisch, M. Head-Gordon, G.W. Trucks, J.B. Foresman, H.B. Schlegel, K. Raghavachari, M.A. Robb, J.S. Binkley, C. Gonzalez, D.J. Fox, R.A. Whiteside, R. Seeger, C.F. Melius, J. Baker, R.L. Martin, L.R. Kahn, J.J.P. Stewart, S. Topiol and J.A. Pople, GAUSSIAN 90 (Gaussian, Inc., Pittsburgh, PA, 1990).
[25] R.A. Kuharski and P.J. Rossky, J. Chem. Phys. 82 (1985) 5164.
[26] J. Lobaugh and G.A. Voth, Chem. Phys. Letters 198 (1992) 311.
[27] H. Azzouz and D. Borgis, J. Chem. Phys. 98 (1993) 7361.
[28] D. Laria, G. Ciccotti, M. Ferrario and R. Kapral, Chem. Phys. 180 (1994) 181.
[29] M.P. Allen and D.J. Tildesley, Computer simulations of liquids (Clarendon Press, Oxford, 1987).

[30] B.R. Brooks, R.E. Bruccoleri, B.D. Olafson, D.J. States, S. Swaminathan and M. Karplus, J. Comput. Chem. 4 (1983) 187.
[31] J. Juanós i Timoneda and J.T. Hynes, J. Phys. Chem. 95 (1991) 10431.
[32] A. Warshel and Z.T. Chu, J. Chem. Phys. 93 (1990) 4003.
[33] D. Borgis, G. Tarjus and H. Azzouz, J. Phys. Chem. 96 (1992) 3198.
[34] D. Borgis, G. Tarjus and H. Azzouz, J. Chem. Phys. 97 (1992) 1390.
[35] D. Laria, G. Ciccotti, M. Ferrario and R. Kapral, J. Chem. Phys. 97 (1992) 378.
[36] D. Borgis, S. Lee and J.T. Hynes, Chem. Phys. Letters 162 (1989) 19.
[37] J. Lobaugh and G.A. Voth, J. Chem. Phys. 100 (1994) 3039.
[38] R. Pomès and B. Roux, manuscript in preparation.